Construction and Building Materials 406 (2023) 133312

Contents lists available at ScienceDirect

Construction and Building Materials

journal homepage: www.elsevier.com/locate/conbuildmat

# Rapid early age strength development of in-line activated geopolymer for concrete 3D printing

Shravan Muthukrishnan [a,b,*], Sayanthan Ramakrishnan [a,c], Jay Sanjayan [a]

[a] Centre for Sustainable Infrastructure and Digital Construction, School of Engineering, Swinburne University of Technology, Hawthorn, Australia
[b] Institute of Construction Materials, Technische Universität Dresden, Dresden, Germany
[c] Centre for Future Materials, School of Engineering, University of Southern Queensland, Springfield, QLD 4300, Australia

ARTICLE INFO

*Keywords:*
Buildability
Pumpability
Set-on-demand
Alkali Activated Concrete
Hydrated Lime
Interlayer bond strength

ABSTRACT

The in-line activation using print head mixing technology involves two parts pumping and mixing at the print head. This technology can be applied in geopolymer concrete, where the base mix (precursors, sand and water) and alkaline activators can be pumped as two separate parts and mixed at the print head for activation. While such methods provide prolonged open time, the early age strength development is low since water from the base mix dilutes the activator solution during print head mixing. Besides, choosing an activator solution with high alkalinity to combat the dilution effect reduces the immediate static yield strength development after print head mixing, which is essential for rapid building. Therefore, this study investigates the hydrated lime as an additive in the base mix to overcome the challenge to attain high 1-day compressive strength along with immediate static yield strength development. The effect of hydrated lime dosage on the pumpability (i.e. evolution of viscosity with time), static yield strength development after print head mixing (buildability) and hardened properties were assessed. The optimum hydrated lime dosage of 1 wt% of the precursors exhibited 1-day compressive strength of 20 MPa and static yield strength of 38.8 kPa after 5 min from print head mixing with minimal changes in pumpability of the base mix for up to 6 h. Moreover, the effect of rapid static yield strength development of the printed layers on the interlayer bond strength was assessed with varying cycle times between 5 s and 40 min. It was found that the interlayer bond strength reduced by 63% when the cycle time was increased from 5 s to 40 min, however, the reduction can be decreased to 15% by surface wetting of the previous layers.

## 1. Introduction

3D concrete printing (3DCP) is a digital construction method that utilises construction scale 3D printers to deposit fresh mix layer by layer to build a designed structure [1]. This construction method does not require formwork, therefore, precise control of the rheology is required for the printable mixes. For instance, the mix should have low viscosity and yield strength during pumping, however, after deposition, the mix should exhibit high viscosity and yield strength to sustain weight from the subsequent layers without significant deformation (buildability). The most commonly studied method to meet this requirement is by adding thixotropic additives during the initial mixing of concrete [2]. However, this method will only increase the thixotropic properties of concrete which has very limited enhancement in buildability. While the high dosage of thixotropic additives may further increase the thixotropy and hence, buildability, it will have a negative impact on the pumpability. A trade-off between pumpability and buildability exists with increasing the thixotropic additives in concrete and therefore, a limited enhancement in buildability can be achieved. In this regard, a relatively new strategy was developed, known as set-on-demand in concrete, to attain the buildability enhancement without affecting the pumpability of the concrete. In this strategy, the concrete with high open time is pumped to the print head and is activated using chemical or thermal intervention to enhance the buildability. As the buildability (measured as yield strength and viscosity) is enhanced at the print head, it does not affect the pumpability of the concrete. In cementitious mixes, chemical interventions using set accelerators are widely studied to attain the on-demand setting of concrete [3,4]. These accelerators are mixed with the concrete at the print head using dynamic [2,4,5] or static mixers [6,7]. Besides, a post-processing method of spraying the accelerator on the

* Corresponding author at: Centre for Sustainable Infrastructure and Digital Construction, School of Engineering, Swinburne University of Technology, Hawthorn, Australia.
*E-mail address:* smuthukrishnan@swin.edu.au (S. Muthukrishnan).

https://doi.org/10.1016/j.conbuildmat.2023.133312
Received 5 July 2023; Received in revised form 5 September 2023; Accepted 9 September 2023
Available online 21 September 2023

printed layer was studied to avoid sophisticated print head mixers [8]. However, spraying the accelerator on the surface of the printed layer leads to non-uniform hardening of the layers (i.e. surface hardens faster than the bulk, which may lead to differential shrinkage in the layers). Ramakrishnan et al. [9] and Shao et al. [10] introduced a new method of encapsulating the accelerator using thermally responsive coatings and mix them during the initial mixing of concrete. This ensures the uniform distribution of the accelerator in the concrete, however, the accelerator does not react with the cement due to the presence of encapsulation. Therefore, the pumpability of the concrete is not affected with the presence of encapsulted accelerator. The print head is attached with a heating medium which dissolves the encapsulation and releases the accelerator. After that, the accelerator reacted with cement to enhance the buildability of the concrete. This ensured uniform hardening of the printed layer without the need for sophisticated print head mixers. Nevertheless, the studies used capsules in the range of a few mm to encapsulate the accelerator, which may cause localised hardening of the print layer. Therefore, the strategy needs to be further investigated to clearly understand the benefits and its feasibility in large scale construction.

Cementitious printable mixes have raised concerns due to the high cement content in the mix and its negative impact on the environment [11]. Therefore, significant attention is gained in alternate printable mixes such as geopolymer concrete that completely replaces cement with alternative cementitious materials [12–14]. While geopolymers increase the sustainability of 3DCP, they restrict the application of set accelerators to attain the on-demand setting of the mix after the deposition. This is due to the incompatibility between the currently available set accelerators and the geopolymers [2].

In this regard, various technologies were investigated to attain the on-demand setting in geopolymer concrete. For instance, Muthukrishnan et al. [15] studied the microwave heating method to instantly accelerate the reaction kinetics of geopolymer at the print head. While the prototype test results were promising, the development of a print head with microwave generators can be quite challenging due to occupational health and safety (OHS) regulations. In another investigation by the authors, the set-on-demand geopolymer mix was attained by in-line activation of the precursors at the print head. In these studies, the precursors were pumped in either dry [16] or liquid form [17] to the print head and were activated using alkaline activators. These set-on-demand geopolymer mixes exhibited high pumpability (long open time) as they were not activated until they reached the print head. In addition, the mix exhibited rapid growth in static yield strength after the print head activation, resulting in enhanced buildability. However, the precise pumping of dry mix ingredients (precursors, aggregates and fibres) to a moving print head is difficult and limits the application of the dry form [16] in large-scale construction. On the other hand, the liquid form proposed in the study [17] is a feasible method to implement on a large scale as the precise pumping of the precursor slurry to the print head can be easily achieved. It is worth noting that this approach is similar to the established set-on-demand approach for cementitious mixes, where set accelerators are injected into the print head. Although the liquid form provides many advantages, the total water content reached was 67 wt% of the precursor (water/binder ratio of 0.67) after the activation of the base mix at the print head, resulting in low early age hardened properties (i.e. 1-day strength) [17]. Such high water content in the printed layers will also lead to detrimental effects on the long-term properties. The primary reason for reduced early age strength properties is that the $Na_2O$ concentration ($Na_2O/H_2O$) in the activator solution significantly reduces during the activation as the water from the base mix dilutes the activator solution. To overcome this issue, the authors utilised superplasticisers to reduce the water content required to prepare the base mix. While the increment in the hardened properties was marginal, a high dosage of SP introduced bleeding in the base mix. The alkalinity of the activator solution ($Na_2O/H_2O$) can also be increased by increasing the percentage of $Na_2O$ in the activator solution. However, this reduces the silicate modulus of the activator solution ($SiO_2/Na_2O$) which, in return, reduces the early static yield strength development of the geopolymer concrete that is vital for set-on-demand mixes [17].

Previous studies have reported that the addition of hydrated lime enhances the early age as well as the long-term strength properties of alkali-activated slag and geopolymers [18–21]. For instance, He et al. [21] stated that the addition of hydrated lime up to 5 wt% of the precursors significantly increased the strength of the geopolymer mix. However, further increment in the hydrated lime dosage reduced the strength but aided in reducing the drying shrinkage. In another study, Shi et al. [18] found that the hydration reaction was significantly enhanced with the addition of hydrated lime for geopolymers containing slag and fly ash. Hydrated lime is a source of calcium ions, which react with silicate anions from the activator solution to produce C-S-H gel thus increasing the strength of the geopolymer mix [21]. Moreover, the reaction between hydrated lime and sodium silicate (the activator) produces sodium hydroxide as a by-product, which increases the alkalinity of the mix [18,19]. This accelerates the dissolution of precursor particles aiding in the strength development. However, excessive hydrated lime content could cause dispersion issues and the unreacted hydrated lime will remain in the form of portlandite crystals. This results in a porous interface between the crystal and matrix, thus reducing the mechanical performance. The reduction in the dormant period that corresponds to the acceleration in hydration reaction in geopolymer was due to the rapid dissolution of $Ca^{2+}$ from slag particles followed by C-S-H formation. Therefore, the addition of hydrated lime at the right dosage could be useful in solving the issues related to early static yield strength development and hardened properties of the set-on-demand geopolymers.

The hydrated lime can also be advantageous to enhance the water reducing effect of superplasticisers (SP). The water-reducing effect of SP is related to the adsorption of SP molecules on the surface of precursors [22]. This includes the surface coverage of precursors with SP and its binding strength. Polycarboxylic ether (PCE) based SPs were reported to be compatible with GGBS, as $Ca^{2+}$ present in the GGBS binds with the carboxylic chain of the SP molecules through a process known as chelation [22]. It is important to note GGBS not only contains $Ca^{2+}$ ions but also other ions in the oxide form. Therefore, the GGBS particle will not be fully covered by SP molecules, decreasing the water-reducing effect of SP. On the other hand, hydrated lime has a significantly higher calcium content than GGBS leading to the enhancement of the water-reducing effect of SP. This may result in a need for a lower SP dosage in the base mix. Hence, the problems related to high SP dosage, such as bleeding of the mix, can be mitigated.

Print head activation of the base mix defines a new method of geopolymer production with the advantages of high open time and rapid static yield strength development after activation. In traditional geopolymer preparation, the activation of precursors is performed during the initial wet mixing of geopolymer concrete. In addition, the mixing duration ranges between 4 and 20 min as per the precursors and type of activators [23–25]. In the print head activation, the dry ingredients (precursors, additives, aggregates and fibres) are mixed with water to produce a base mix. The base mix is then mixed with an alkaline solution at the print head for a short duration (i.e. 15–60 s) to produce geopolymer concrete. Here, the hydrated lime can either be introduced in the base mix or as another input at the print head. While the former technique may reduce the open time of the base mix due to the mild activation by hydrated time, the latter method will lead to high water content in the mix due to the requirement of hydrated lime supplied in slurry form. In this study, the hydrated lime is introduced in the initial mix slurry at specified dosages and the properties of geopolymer after activation is studied. In this regard, the effect of hydrated lime and SP on the fresh and hardened properties of geopolymer may change with the new mixing regime and needs to be understood. For instance, the optimum hydrated lime dosage of 5 wt% of precursor identified by He et al. [21] might vary for set-on-demand geopolymer mix developed by print

head activation of the base mix.

With the concerns mentioned above, this study first identifies the effect of hydrated lime to mitigate the early static yield strength reduction in the geopolymer mix activated using a low silicate modulus alkaline solution. Once the optimum hydrated lime dosage is identified, the mix is further modified with the incorporation of PCE-based SP to enhance the mix's fresh and hardened properties for 3DCP. While the rapid setting of the mix is beneficial for buildability, it can be detrimental to the interlayer properties. Therefore, the optimised set-on-demand mix with hydrated lime and SP is assessed for interlayer bond strength at various cycle times.

## 2. Materials and methods

### 2.1. Precursors, additives and aggregates

Precursors used to prepare geopolymers in this study were Ground Granulated Blast Furnace Slag (referred to as slag hereafter) and class F fly ash. The slag, complying with AS 3582.1, was supplied by Independent Cement and Hydrated lime Pty Ltd., Australia, whereas the fly ash, complying with AS 3582.1 was supplied by Cement Australia Pty Ltd., Australia. Hydrated lime with a purity of 95 wt% was used to improve the early-age static yield strength of the mix. The geopolymer precursors were activated using a sodium silicate solution with a silicate modulus of 2.0. The silicate modulus is defined as the molar ratio between the $SiO_2$ and $Na_2O$ content in the sodium silicate solution. The sodium silicate solution was supplied by PQ Australia Pty. Ltd., Australia. The sodium silicate solution composes of 14.70 wt% $Na_2O$, 29.4 wt% $SiO_2$ and 55.9 wt% water. The density and pH of the solution are 1.53 g/cm$^3$ and 12.7 respectively [26].

Three types of sand, identified as Coarse sand (CS), Medium sand (MS) and fine sand (FS), were used as fine aggregates for geopolymer concrete. All the types of sand were supplied by Holcim Australia. The coarse sand has a maximum particle size of 1.7 mm, whereas medium sand and fine sand have a maximum particle size of 0.71 mm and 0.36 mm respectively. The D10 (10% of particles passing through) of CS, MS and FS was 0.46 mm, 0.32 mm and 0.06 mm respectively. The corresponding D50 were 0.64 mm, 0.4 mm and 0.14 mm and D90 were 0.92 mm, 0.48 mm and 0.2 mm respectively.

### 2.2. Preparation of geopolymer mix

Table 1 shows the mix design of the geopolymer investigated in this study. The sand-to-precursor ratio was kept the same for all the mixes at 1.5:1. Similarly, the activator-to-precursor ratio was kept constant at 0.35: 1 for all the mixes. Mixes from 0.8S-0.42W to 0.715S-0.42W-0.085CH contain 20 wt% of the precursors as fly ash and the rest as slag and hydrated lime. In the case of mixes from 0.5S-0.38W to 0.415S-0.38W-0.085CH, the fly ash content was increased to 50 wt% of the precursors. In the previous study [17], the fly ash dosage was varied from 10 wt% to 50 wt% of the precursors to understand the effect of various fly ash dosages on the static yield strength development with time of the geopolymer concrete. It was determined that the mix with 20 wt% fly ash showed the maximum growth in static yield strength after 25 min from the print head mixing. Therefore, a fly ash dosage of 20 wt % was selected in this study to compare the results with the set-on-demand mix reported in Ref. [17]. Meanwhile, other studies [16,27,28] have reported that a fly ash dosage of 50 wt% exhibits good hardened properties and durability, therefore a fly ash dosage of 50 wt% of precursors was also considered.

The mixes with high fly ash content required less water to maintain the required workability, therefore the W/B for mixes from 0.5S-0.38W to 0.415S-0.38W-0.085CH was 0.38. Meanwhile, W/B of 0.42 was used for preparing mixes from 0.8S-0.42W to 0.715S-0.42W-0.085CH. As the hydrated lime is a source of $Ca^{2+}$ like slag, the hydrated lime was incorporated into the mix by partially replacing slag from 0 wt% to 8.5 wt% of the precursors. The preparation method of the mixes is as follows: Dry ingredients after measuring were transferred to a planetary (Hobart) mixer and mixed for a minute at 60 rpm. After that, the water was added to the dry mix and the wet mixing was conducted for 3 min and 30 s. The first 2 min of wet mixing was conducted at 60 rpm, which was followed by mixing at high speed (124 RPM) for 1 min and 30 s. Before changing the mixing speed, the material adhered to the surface was scrapped and blended with the mix. The mix obtained is referred to as the base mix and its rheology governs the pumpability of the set-on-demand geopolymer mix. The base mix was then mixed with the activator solution for 30 s at 124 rpm. This represents the in-line activation of the base mix at the print head. The fresh concrete obtained after print head mixing was used to determine the buildability and hardened properties. A similar mixing regime was used in the authors' previous study [17] to simulate the inline activation of the precursor slurry (base mix) in the print head.

## 3. Experimental programme

### 3.1. Identifying optimum hydrated lime dosage

#### 3.1.1. Evolution of static yield strength with time

As stated earlier, hydrated lime is investigated to enhance the early-age buildability of the geopolymer mix. Therefore, the evolution of static yield strength with time was determined for geopolymer mixes with various hydrated lime dosages. A slow continuous penetration test was used to determine the static yield strength development of the mixes [16]. The base mix after activation was transferred to the sample holder

**Table 1**
Mix design of the geopolymers investigated.

| Mix ID | Precursors | | | Aggregate | | | Water/Precursor (in the base mix) | Activator/ Precursors | Water/Precursors (After activation) |
|---|---|---|---|---|---|---|---|---|---|
| | Slag | Fly ash | Hydrated lime | Coarse Sand | Medium Sand | Fine Sand | | | |
| **0.8S-0.42W** | 0.8 | 0.2 | 0 | 0.5 | 0.5 | 0.5 | 0.42 | 0.35 | 0.62 |
| **0.79S-0.42W-0.01CH** | 0.79 | | 0.01 | | | | | | |
| **0.75S-0.42W-0.05CH** | 0.75 | | 0.05 | | | | | | |
| **0.715S-0.42W-0.085CH** | 0.715 | | 0.085 | | | | | | |
| **0.5S-0.38W** | 0.5 | 0.5 | 0 | | | | 0.38 | | 0.58 |
| **0.49S-0.38W-0.01CH** | 0.49 | | 0.01 | | | | | | |
| **0.45S-0.38W-0.005CH** | 0.45 | | 0.05 | | | | | | |
| **0.415S-0.38W-0.085CH** | 0.415 | | 0.085 | | | | | | |

and a conical needle was slowly immersed into the fresh concrete at 10 mm/h using a universal testing machine. The conical needle was connected to a 500 N load cell that has an accuracy of 0.15 N. The resistance of penetration was recorded with time and converted to the static yield strength. The experimental setup including the needle dimensions is explained in detail in the authors' previous study [17].

#### 3.1.2. Compressive strength at 1, 7 and 28 days

The effect of hydrated lime on the hardened properties of the geopolymer mix was studied by determining the compressive strength for mould-cast specimens prepared using geopolymer mixes with various hydrated lime dosages at 1, 7 and 28 days. The fresh mix was cast into 50 mm X 50 mm X 50 mm moulds for assessing the compressive strength. After casting, the fresh mix was sealed and kept in the environmental-controlled chamber, operating at 25°C and 65% relative humidity, for 24 h. The specimens were then de-moulded and kept in the same environment-controlled chamber without sealing until the test date. Three samples for each hydrated lime dosage and age were tested. The average compressive strength was then reported with one standard deviation.

#### 3.1.3. Pumpability of the base mix

Once the optimum hydrated lime dosage exhibiting the highest buildability and hardened properties was chosen from the earlier sections, it was tested for pumpability. Hydrated lime has been used as an activator in previous studies [29,30]. Therefore, even though the base mix is not activated with the primary activators, the hydrated lime can activate the geopolymer precursors and reduce the pumpability of the base mix with time. In addition, slag shows cementitious properties, hence, can react with water to form hydration products, which in turn increases the viscosity of the mix [31]. Therefore, two mixes were chosen each from the 20% slag group and 50% slag group and they were subjected to the rheological assessment to test the mix's pumpability.

A rotational rheometer with a 6-blade vane and cup was used to determine the apparent viscosity (rheological parameter). The base mix after preparation was transferred to the cup and sheared according to the shearing protocol shown in Fig. 1. The base mix was first pre-sheared at 80 rpm for 60 s to alleviate the effect of shearing history on the apparent viscosity. After that, the base mix was sheared from 0 rpm to 80 rpm in 8 steps and back to 0 rpm in 8 steps, referred to as the ramping-up and the ramping-down section of the shearing protocol respectively. The shearing at each step was continued for 30 s to ensure the torque obtained at each step reaches a steady state. The torque corresponding to each step was determined by averaging the torque values measured in the last 5 s of the step. The average torque was then plotted against the corresponding shearing rate (RPM) to get the flow curve. Consequently, the apparent viscosity was measured using the Reiner-Riwlin equation for each shearing rate applied during the ramping-down section of the flow curve [32]. The apparent viscosity was measured for different resting durations varying from 0 h to 6 h. The resting duration of the mixes was ensured by keeping the base mix after pre-shearing at rest inside the rheometer cup for a pre-defined duration (0 h to 6 h) before the measurement. The cup was sealed during the resting duration to avoid significant moisture loss. It is worth mentioning that the multi-batch approach was used to measure the evolution of apparent viscosity with time. That means separate batches of the base mix were prepared for each resting duration to measure the apparent viscosity.

### 3.2. Interlayer properties of the set-on-demand geopolymer concrete

#### 3.2.1. Interlayer bond strength

The rapid setting of the geopolymer mix with hydrated lime can influence the malleability of the printed layer, thus affecting the interlayer bond strength of the printed specimen. For instance, if the printed layer has low malleability, it is difficult for the new layer to adhere to the previous layer, resulting in low interlayer bond strength [33]. Moreover, the malleability of the printed layer is related to the cycle time of the printing operation, i.e., the longer the cycle time lower the malleability of the printed layer. Here, cycle time is referred to as the time taken to print a layer of the designed structure. Cycle time varies as per the structure's size, shape and printing speed. Therefore, two-cycle times – 5 s and 40 min were considered for the assessment to cover a wide range of printing operations. A customised printer consisting of a piston-type extruder connected to a 0.45 L rectangular barrel was used to print the specimens for this purpose. The extruder can be operated at 6 different extrusion rates with a maximum pushing force of 4500 Nm. More details on the printer can be found in the authors' previous study [17]. The selected mix from the previous sections was prepared in a Hobart mixer and transferred to the customised printer for printing. Two layers of 300 mm length, 50 mm width and 25 mm thickness were printed. The time interval between the layers was kept at 5 s and 40 min for the assessment. After printing, the specimens were sealed and cured for 24 h at ambient conditions and then kept in the water bath for the rest of the curing duration (i.e., 27 days). After curing, the specimens were cut into 50 mm × 50 mm × 50 mm sections for interlayer bond strength measurement. A 4 mm wide triangular notch was created on both sides of the interlayer to ensure the failure occurs at the interlayer. Six samples for each cycle time were tested and the average interlayer bond strength was reported with one standard deviation.

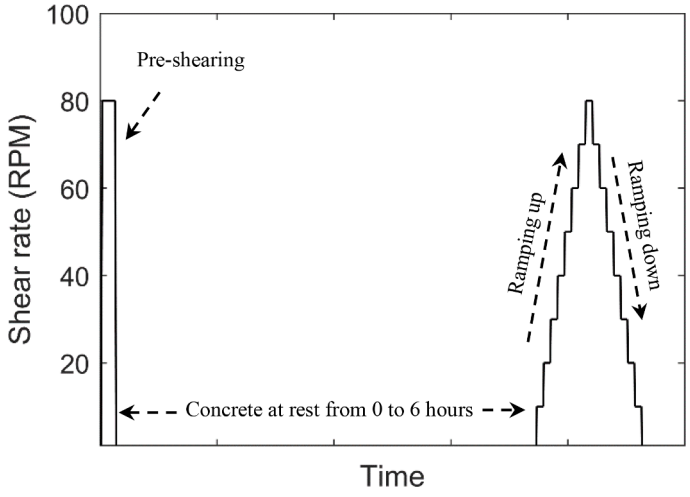


**Fig. 1.** Shearing regime used to determine apparent viscosity.

### 3.2.2. Volume of permeable voids (VPV)

The relationship between the interlayer bond strength and the cycle time was further analysed by determining the volume of permeable voids of the printed specimens according to AS 1012.21–1999. After 28 days of curing, the printed specimens were cut into 50 mm X 50 mm X 50 mm cubes and were heated at 105 °C for 24 h to evaporate the moisture from the pores. The specimens were then cooled down to 25 °C before measuring the dry weight ($W_1$). After that, the samples were boiled in water to saturate the pores with water. The boiling was stopped after 5.5 h, and the samples were left in the water until the temperature reached 25 °C. Then, the samples were removed and the excess water on the surface was wiped using a tablecloth before measuring the weight ($W_2$). Subsequently, the samples were suspended in the water using a metal cage to measure the suspended weight ($W_3$). The measured weights were then inserted into equation (1) to determine the VPV. The VPV was determined for six samples for each cycle time and the average VPV was reported with one standard deviation.

$$\%Volumeofpermeablevoids(VPV) = \frac{W_2 - W_1}{W_2 - W_3} X100 \quad (1)$$

## 4. Results and discussion

### 4.1. Effect of hydrated lime dosage on the fresh and hardened properties of 3D printable concrete

Fig. 2 and Fig. 3 show the static yield strength development of the mixes with various hydrated lime dosages. Mixes represented in Fig. 2 contain 20 wt% of the precursors as fly ash, whereas Fig. 3 depicts the mixes containing 50 wt% of the precursors as fly ash. Interestingly, the hydrated lime dosage of 1 wt% of precursors exhibited maximum static yield strength development with time regardless of the slag to fly ash ratio. Hydrated lime is a source of $Ca^{2+}$ ions that reacts with silicates from the activator to form C-S-H which increases the static yield strength of the mix [21]. In addition, the hydrated lime ($Ca(OH)_2$) increases the alkalinity of the mix, accelerating the dissolution of the precursors. However, according to Fig. 2(a) and Fig. 3(a), the static yield strength development reduced with the increment in the hydrated lime dosage beyond 1 wt% of the precursors. Most of the mixes with hydrated lime dosage above 1 wt% of the precursors showed slower static yield strength development than the mix without hydrated lime, especially in the early stage. To understand this contradictory behaviour, the mixing energy after the introduction of the activator solution was measured using a power meter connected to the Hobart mixer. Fig. 4 shows the variation in power consumption with time after introducing the activator solution to the mixes with 0–8.5 wt% of hydrated lime.

The measured power consumption during the print head mixing process, as depicted in Fig. 4, reveals that the power consumption is constant for a short duration immediately after the addition of activator solution followed by an increase in the power. This short duration (dormant period) varies from 150 s in the mix with no hydrated lime to about 15 s for mixes with hydrated lime. The reduction in this dormant period with the increased hydrated lime dosage suggests the rapid

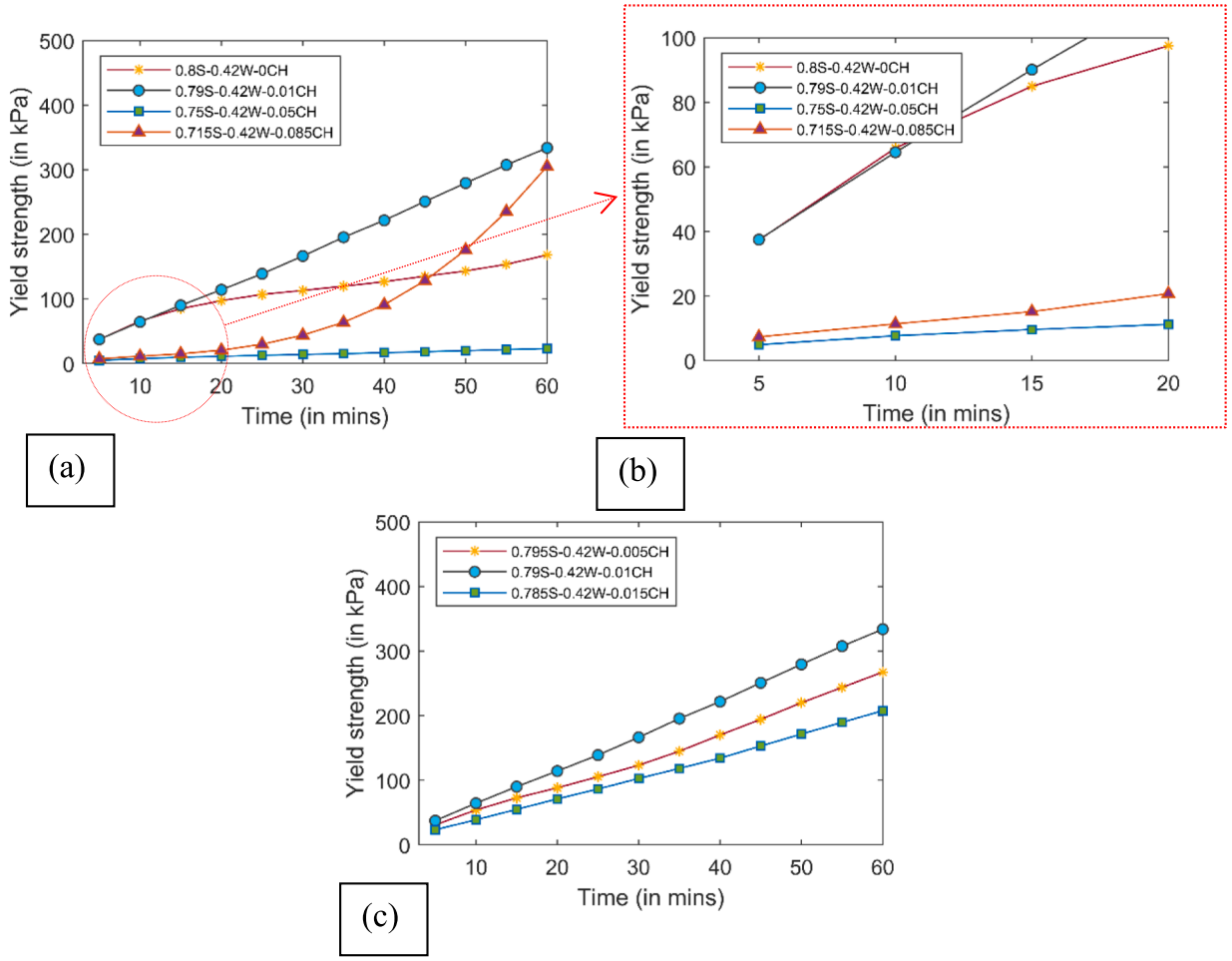


**Fig. 2.** Static yield strength development of geopolymer concrete with 20 wt% of the precursors as fly ash and hydrated lime from 0 to 8.5 wt% of the precursors. Static yield strength until (a) 60 min and (b) 20 min from the activation. (c) Static yield strength development of the mix with the hydrated lime dosage of 0.5 wt%, 1 wt% and 1.5 wt% of the precursors.

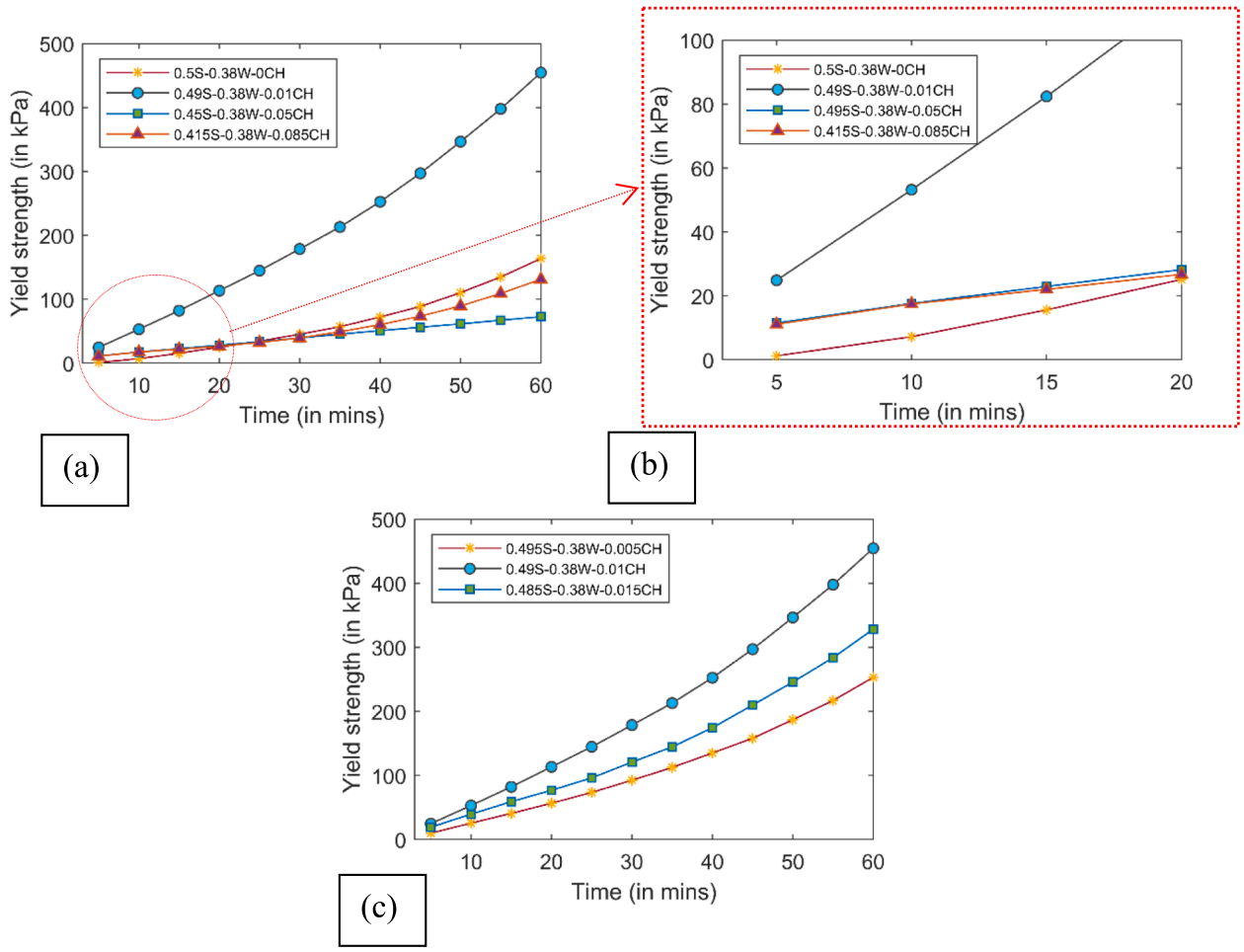


**Fig. 3.** Static yield strength development of geopolymer concrete with 50 wt% of the precursors as fly ash and hydrated lime from 0 to 8.5 wt% of the precursors. Static yield strength until (a) 60 min and (b) 20 min from the activation. (c) Static yield strength development of the mix with the hydrated lime dosage of 0.5 wt%, 1 wt% and 1.5 wt% of the precursors.

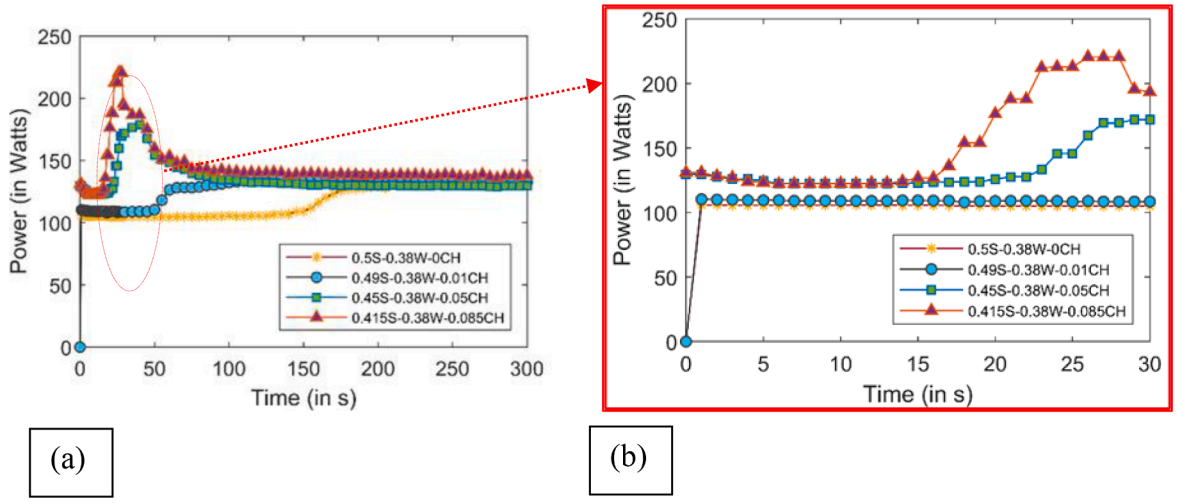


**Fig. 4.** Power consumption measured during the activation of the base mix containing hydrated lime at various dosages (0–8.50%). Print head mixing duration of (a) 300 s and (b) 30 s.

formation of C-S-H. Therefore, the introduction of hydrated lime leads to rapid strength development, thus agreeing with the reported behaviour of hydrated lime with sodium silicate in previous studies [18,19,21].

During the print head activation, the base mix resides in the print head mixer for 30 s after the first contact with the activator solution. For mixes with hydrated lime dosage above 1 wt% of the precursors, the shift in the power consumption corresponding to the C-S-H formation occurred before the 30 s of mixing duration. Therefore, excessive mixing

could have broken the early C-S-H formations, resulting in low static yield strength development of the mix after the deposition. Previous studies have reported that the shearing of early C-S-H delayed the setting rate of the geopolymers [16,34]. This knowledge was also applied in developing one-part geopolymer mixes for 3D printing applications, where the fresh printable mix was obtained after around 20 min of mixing to ensure good pumpability (low setting rate) [23,35]. In those mixes, reducing the mixing duration resulted in the flash setting of the mixes. Meanwhile, for mixes with a hydrated lime dosage of 0 wt% and 1 wt% of precursor, the shift in the power consumption corresponding to the C-S-H formation occurred after 30 s. This resulted in negligible shearing of C-S-H during the print head activation, which resulted in rapid growth in the static yield strength of the mix after the deposition as shown in Fig. 3 and Fig. 4.

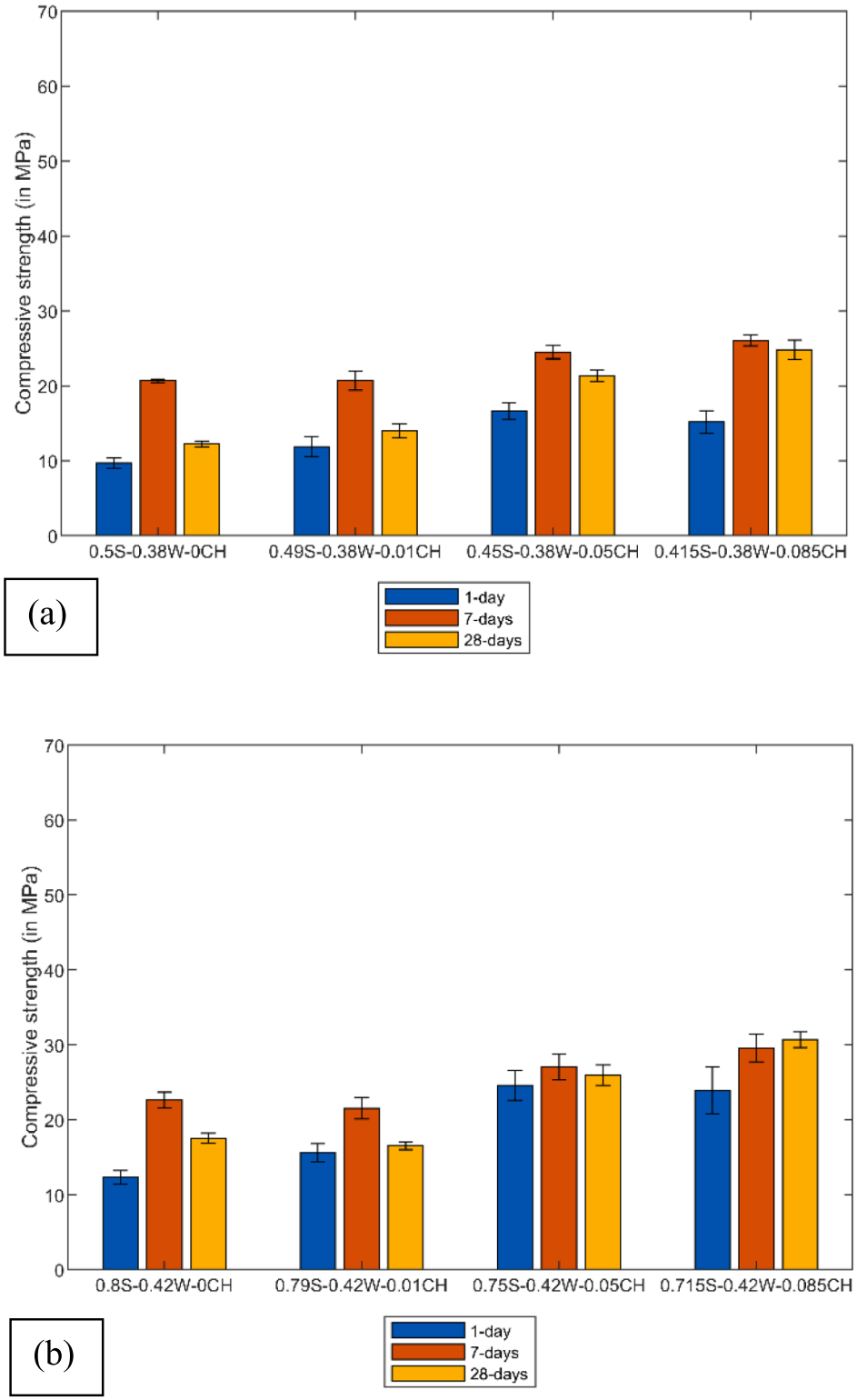


**Fig. 5.** Effect of hydrated lime on the compressive strength of geopolymer mixes cured at ambient conditions. The fly ash dosages used were (a) 50 wt% and (b) 20 wt % of precursors (error bars indicate mean ± one standard deviation).

The influence of shearing of early C-S-H during print head activation was found to be insignificant on the hardened properties of the geopolymers. As shown in Fig. 5, the compressive strength increased with the increment in hydrated lime dosage for both the groups of mixes containing 50 wt% and 20 wt% of precursors as fly ash. The incorporation of hydrated lime increases the Ca/Si of the mix, resulting in higher cross-linking between the hydration products [21]. The cross-linking enhances the density of the geopolymer matrix, resulting in higher compressive strength [36,37]. In addition, the higher hydrated lime dosage in the mix has resulted in a lower reduction of compressive strength from 7 days to 28 days. For instance, according to Fig. 5(a), the compressive strength of the mix with hydrated lime content of 8.5 wt% of precursors was reduced by 4.8% from 7 to 28 days, whereas the compressive strength of the mix without hydrated lime showed a reduction of 41% from 7 to 28 days. This implies high dosages of hydrated lime are beneficial to attain good hardened properties, especially 28-day compressive strength. However, high dosages of hydrated lime resulted in low static yield strength development of the mix after deposition which reduces the buildability of the mix. As the current study focuses on developing set-on-demand geopolymer mixes, the early age static yield strength development is crucial. Therefore, the hydrated lime dosage of 1 wt% of the precursors was selected for further investigation. In the following investigation, the W/B of the mixes is reduced with the incorporation of superplasticiser to enhance the hardened properties without sacrificing the static yield strength development of the mix.

### 4.2. Effect of superplasticiser on 28 days compressive strength

The mixes selected from the previous section, 0.49S-0.42W-0.01CH and 0.79S-0.38W-0.01CH were improved with the introduction of PCE based SP to reduce the water to binder ratio after the activation as shown in Table 2. Therefore, the water to precursor ratio of the base mix was reduced with the addition of superplasticiser as shown in Table 2. It is important to note that the water to precursor ratio can be further reduced by increasing the dosage of superplasticiser. However, further reduction in the water to precursor ratio resulted in quick drying of the mix after the activation. In this context, quick drying is referred to as the sudden loss in the fluidity of the mix to the extent of drying. To prevent the quick drying effect, the water to precursor ratio was kept at 0.26 and 0.28 for mixes containing 50 wt% and 20 wt% of precursors as fly ash respectively. Reduced water to precursor ratio with the addition of superplasticiser significantly enhanced the static yield strength development of the base mix after activation as shown in Fig. 6. For instance, the static yield strength of the mix 0.49S-0.38W-0.01CH was determined as 454 kPa at 60 min, whereas with the addition of SP the corresponding static yield strength was determined to be 868 kPa showing an increase of 92%. For 0.79S-0.42W-0.01CH mix, the static yield strength at 60 min was determined as 334 kPa, whereas the addition of SP has resulted in the increment of corresponding static yield strength by 63%. Importantly, both the mixes exhibited a faster static yield strength development rate than the set-on-demand geopolymer mix developed in Ref. [17] even though the silicate modulus of the activator solution was reduced from 2.68 to 2.00.

Fig. 7 shows the 1-day, 7-day and 28-day compressive strengths of the geopolymer mixes prepared according to Table 2. The 1-day strength was significantly improved with the addition of hydrated lime and activator solution of silicate modulus of 2.0. While the mix reported in Ref. [17] exhibited a 1-day compressive strength of ~ 2 MPa, the addition of hydrated lime and activator solution of silicate modulus of 2.0 increased the 1-day strength by around 10 times. Therefore, the major limitation of the set-on-demand mix attained by the in-line activation of the base mix in Ref. [17] (i.e., low 1-day strength) has been mitigated in this study. 1-day strength is important in 3DCP, especially when the printed structures need to be moved or transported after printing. Having low 1-day strength can be detrimental to the productivity of 3DCP in such cases [17].

Furthermore, the addition of SP showed significant improvement in 1-day, 7-day and 28-day compressive strength compared to the mixes without SP. For instance, when the specimens were kept in ambient conditions, the mixes with SP showed 52% and 72% higher 28-day compressive strength than the mixes without SP (0.79S-0.42W-0.01CH and 0.49S-0.38W-0.01CH respectively). It was observed that the compressive strength of the mixes with SP increased with the age, however after 7-days, the compressive strength was observed to decrease like the mixes without SP. It implies that even though the water-to-precursor ratio was reduced with the addition of SP, the reduction in compressive strength from 7 to 28 days is not eliminated for ambient cured specimens. Moreover, the effect of fly ash dosage was found to be insignificant on the 28-day compressive strength of the mixes with SP. For instance, the average 28-day compressive strength of mixes 0.49S-0.26W-0.01CH and 0.79S-0.28W-0.01CH were 24.1 MPa and 25 MPa respectively. In contrast, the water bath curing method significantly increased the compressive strength of all the mixes as shown in Fig. 7. The effect of fly ash dosage was found to be significant on compressive strength with this curing method. For instance, the mix 0.49S-0.26W-0.01CH exhibited ~ 30% higher compressive strength than the mix 0.79S-0.28W-0.01CH. Moreover, the compressive strength increased from 7 to 28 days with this curing method, contradicting the trend observed for the ambient cured specimens.

### 4.3. Pumpability of the base mix

Fig. 8 represents the evolution of apparent viscosity with time for mixes shown in Table 2. The apparent viscosity of the mix governs the pressure required to pump the base mix to the print head (pumpability). The low viscosity of the mix translates to the low pressure required to pump the mix, thus high pumpability. Fig. 8 implies that the evolution of viscosity with time is sensitive to precursor composition. For the mix 0.79S-0.28W-0.01CH, the apparent viscosity increased significantly with time, even though the base mix was not activated. This could be due to both the absorption of water by the dry ingredients and the cementitious properties of slag and hydrated lime, which involves the dissolution of $Ca^{2+}$ into the pore solution followed by the formation of $Ca(OH)_2$. But, according to Fig. 8 (a), the latter was more pronounced in this case. Fig. 8(a) shows the evolution of viscosity with time of the mix 0.49S-0.26W-0.01CH. It was found that the apparent viscosity was between 4 and 10 Pa.s for 6 h of resting duration. In the case of the mix 0.79S-0.28W-0.01CH, the apparent viscosity increased from 6 Pa.s to 200 Pa.s within the 6 h of resting duration (Fig. 8(b)). As both the mixes

**Table 2**
Mix designs used in section 4.2.

| Precursors | | | Aggregates | | | Water/Precursors (in the base mix) | Activator/ Precursors | SP (ml) | Water/ Precursors (After activation) |
|---|---|---|---|---|---|---|---|---|---|
| Slag (kg) | Fly ash (kg) | Hydrate hydrated lime (kg) | Coarse sand (kg) | Medium Sand (kg) | Fine sand (kg) | | | | |
| 0.79 | 0.2 | 0.01 | 0.5 | 0.5 | 0.5 | 0.28 | 0.35 | 4 | 0.48 |
| 0.49 | 0.5 | 0.01 | 0.5 | 0.5 | 0.5 | 0.26 | 0.35 | 4 | 0.46 |

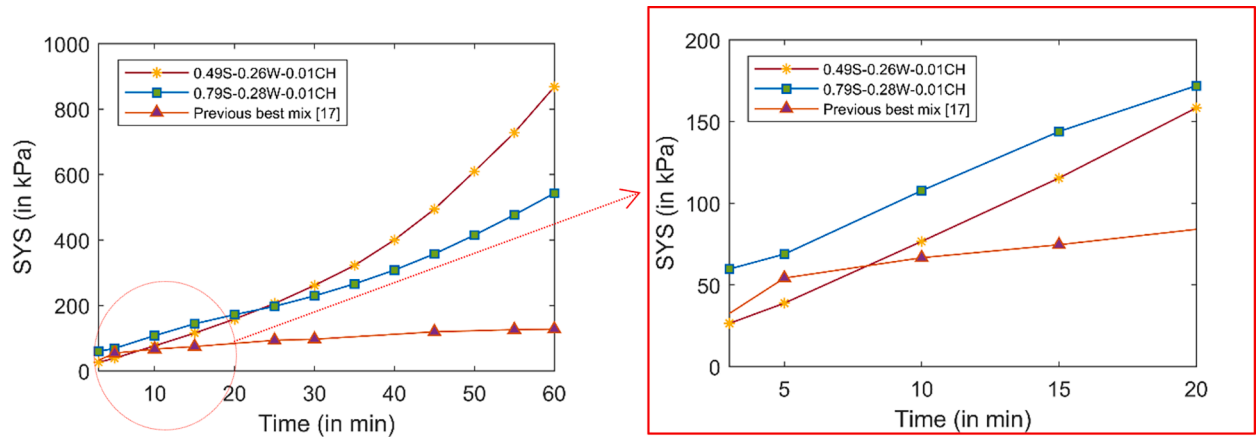


**Fig. 6.** Static yield strength development of geopolymer mixes shown in Table 2 and the mix reported in Ref. [17].

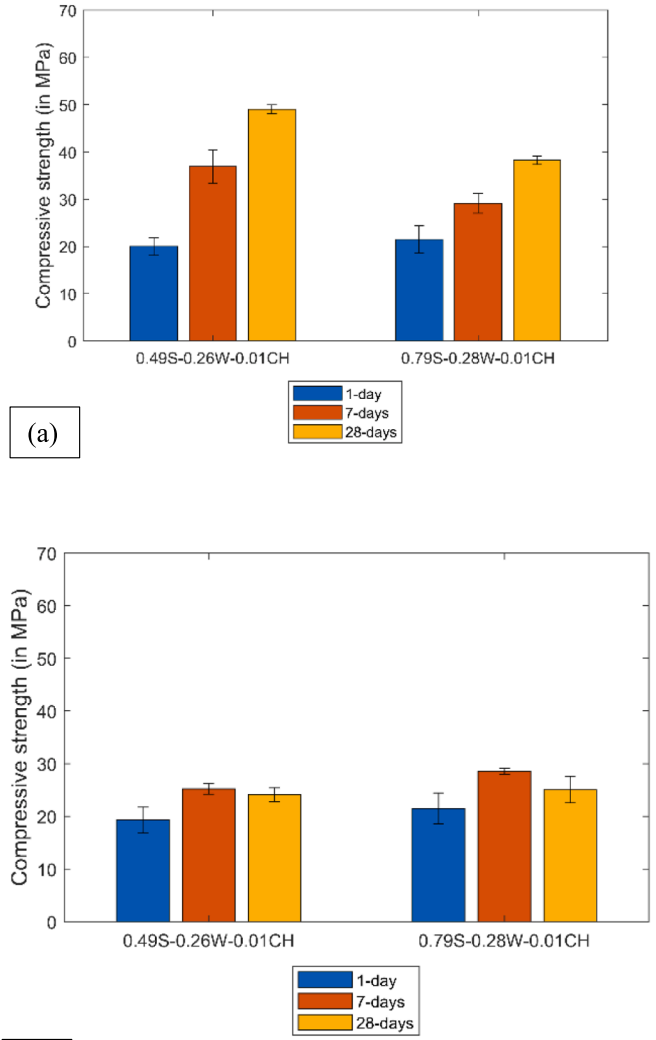


**Fig. 7.** Compressive strength of geopolymer mixes (shown in Table 2) cured in (a) water bath and (b) ambient conditions (error bars indicate mean ± one standard deviation).

have the same amount of sand that majorly contributes to water absorption, it can be said that the difference in the viscosity development between the mixes is due to the cementitious properties of precursors.

Even though both the mixes are not activated, the slag and hydrated lime can dissolve into the pore solution and increase the alkalinity. This further enhances the dissolution rate of the precursors. This process is slow, and the dissolution rate is governed by the amount of slag and hydrated lime present in the base mix. For the mix 0.49S-0.26W-0.01CH (shown in Fig. 8(a)), the amount of slag is low, hence, the dissolution rate of $Ca^{2+}$ to the pore solution is low. This resulted in marginal evolution of apparent viscosity with time for this mix. However, in the case of the mix 0.79S-0.28W-0.01CH (shown in Fig. 8(b)), the amount of slag was 60% higher than the mix 0.49S-0.26W-0.01CH. This resulted in the faster dissolution of $Ca^{2+}$ ions into the pore solution, which in turn enhanced the evolution of the apparent viscosity of the base mix with time. Moreover, a higher amount of round-shaped fly ash particles was also attributed to the low viscosity of the mix 0.49S-0.26W-0.01CH due to the ball-bearing effect [38].

The comparison of various fresh and hardened properties of chosen optimum mixes from 50% FA and 20% FA groups is given in Table 3. With regards to the pumpability of base mixes determined by the evolution of apparent viscosity with time, the mix 0.49S-0.26W-0.01CH performed better than the mix 0.79S-0.28W-0.01CH. Similarly, the compressive strength of the mix 0.49S-0.26W-0.01CH was found to be higher than the mix 0.79S-0.28W-0.01CH (Table 3). Meanwhile, in the case of static yield strength development, the mix 0.79S-0.28W-0.01CH showed higher static yield strength development than the mix 0.49S-0.26W-0.01CH (Table 3). However, after 20 min of activation, the static yield strength of the mix 0.49S-0.26W-0.01CH exceeded the mix 0.79S-0.28W-0.01CH. It is worth noting that although the early static yield strength development of the mix 0.49S-0.26W-0.01CH was lower than the mix 0.79S-0.28W-0.01CH, the mix 0.49S-0.26W-0.01CH exhibited a static yield strength of 38.8 kPa at 5 min after activation. This translates to a buildability of a 3.6 m tall structure according to Ref. [39]. Therefore, the mix 0.49S-0.26W-0.01CH was used for further investigation.

### 4.4. Interlayer bond strength of set-on-demand geopolymer concrete

The interlayer bond strength of developed set-on-demand concrete was investigated to assess the effect of rapid setting of geopolymers causing poor malleability during the printing. The inadequate malleability of fresh layers will lead to poor mechanical bonding between layers and forms cold joints. This effect is further exacerbated by the increased cycle time between printing. Therefore, to consider these effects, two printing scenarios of cycle times at 5 s and 40 min between layers is investigated and the corresponding interlayer bond strength results are depicted in Fig. 9. As expected, the interlayer bond strength reduced with the increment in cycle time. For instance, when the cycle time was increased from 5 s to 40 min, the interlayer bond strength was

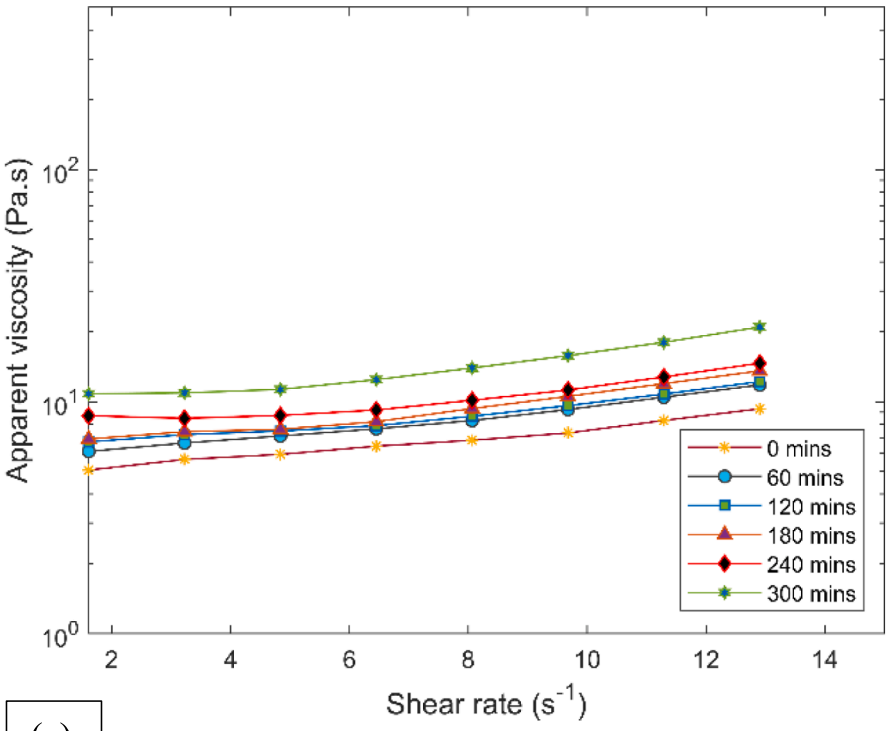


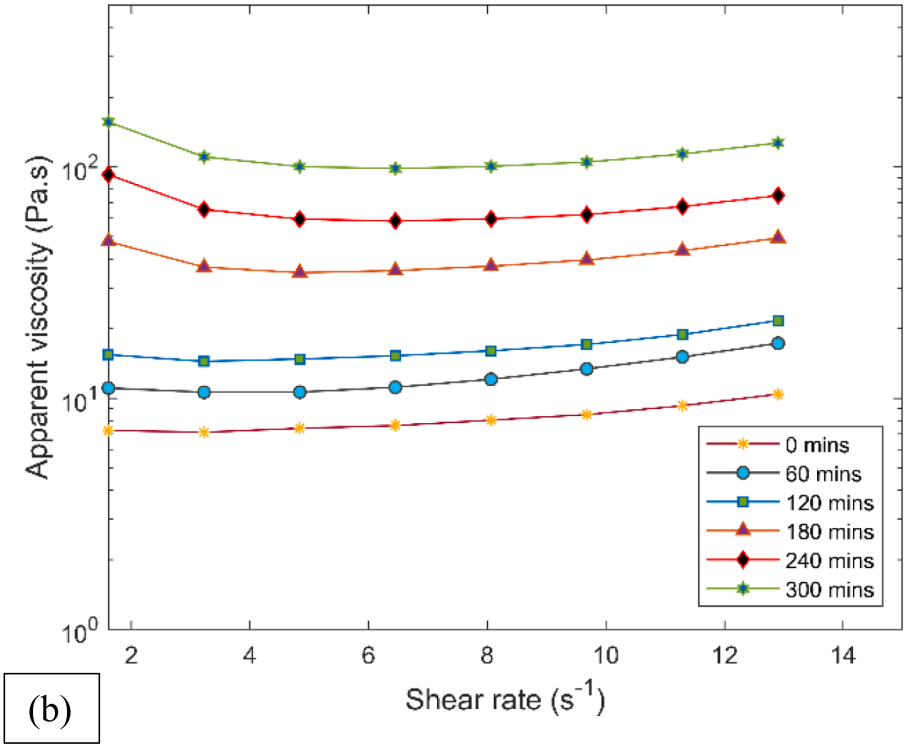


**Fig. 8.** Evolution of apparent viscosity with time for mixes containing (a) 50 wt% and (b) 20 wt% of precursors as fly ash.

**Table 3**
Comparison between mixes 0.49S-0.26W-0.01CH and 0.79S-0.28W-0.01CH.

| Properties | 0.49S-0.26W-0.01CH | 0.79S-0.28W-0.01CH |
|---|---|---|
| **Compressive strength (hardened properties)** | | |
| 1 day | 20.02 MPa | 21.51 MPa |
| 7 day | 36.94 MPa | 29.14 MPa |
| 28 day | 49.05 MPa | 38.24 MPa |
| **Static yield strength (Fresh properties - buildability)** | | |
| Up to 20 min | 26.4 kPa to 158.4 kPa | 59.7 kPa to 171.9 kPa |
| 20 min to 60 min | 158.4 kPa to 867.9 kPa | 171.9 kPa to 542.8 kPa |
| **Viscosity (Fresh properties – Pumpability)** | | |
| After 6 h | In the order of 10 Pa.s | In the order of 100 Pa.s |

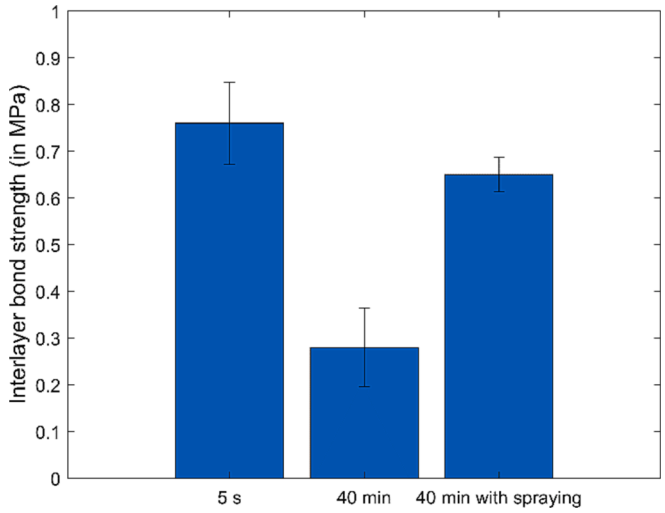


**Fig. 9.** Interlayer bond strength of the printed specimens at various cycle times (error bars indicate mean ± one standard deviation).

reduced by 63 %.

After 40 min, the printed layer had a static yield strength of ~ 400 kPa (Fig. 6) which is equivalent to a compressive strength of ~ 1 MPa [39]. Therefore, the malleability of the printed layer was very low for effective bonding of the printed layer with the new layer. Moreover, a longer cycle time exposes the (top) surface of the printed layer for longer drying before stacking. This reduces the surface moisture content and increases the shrinkage which contribute to the porous interlayer. Many previous studies have studied the effect of surface moisture on the interlayer bond strength [40–42]. The change in surface moisture is mostly due to bleeding and evaporation of water from the surface, influencing the interlayer bond strength. Therefore, a surface preparation method was followed, where the surface of the previously printed layer was sprayed with water until saturation shortly before depositing the new layer. It is worth mentioning that spraying was only performed for printed specimens with 40 min cycle time. Printed specimens with 5 s cycle time did not require spraying water before depositing the new layer because the previous layer was malleable and moist enough after 5 s. As shown in Fig. 9, the interlayer bond strength was increased by 130% when the water was sprayed shortly before the deposition of the new layer. Most likely, when a new layer is deposited on a dry (previous) layer, it absorbs moisture from the new layer. This increases the porosity of the new layer especially at the interlayer, resulting in effective bond area reduction, hence low interlayer bond strength.

This hypothesis was validated by measuring the volume of permeable voids of the printed specimens. As the mix design and curing conditions were the same for all the printed specimens, the change in porosity with the cycle time can be related to the interlayer. It was found that the VPV follows the same trend with cycle time as the interlayer bond strength (Fig. 10). When the cycle time was increased from 5 s to

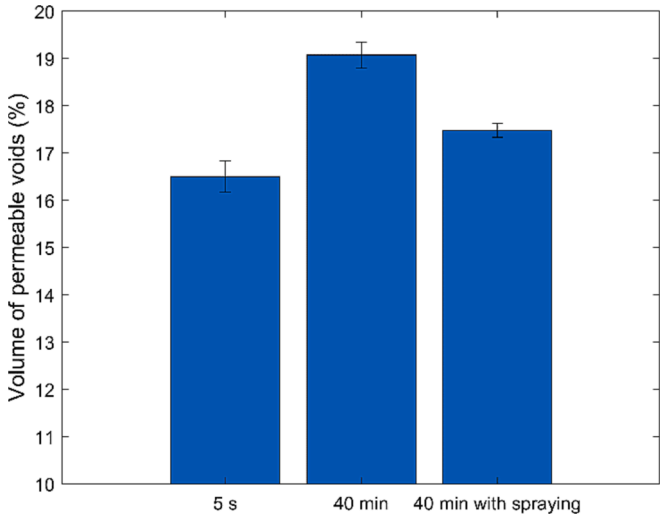


**Fig. 10.** Volume of permeable voids of the printed specimens prepared at different cycle times (error bars indicate mean ± one standard deviation).

40 min, the VPV of the printed specimens was increased by 13.3%. In addition, spraying of water shortly before the deposition of the new layer reduced the VPV of the printed specimens (with 40 min cycle time) by 8.4%. Therefore, it can be concluded that the surface moisture of the previously deposited layer controls the porosity of the interlayer which in turn governs the interlayer bond strength. However, it is important to note that the interlayer bond strength after spraying water was still 15% lower than the printed specimen with 5 s cycle time. This is due to the low malleability of the previously deposited layer and spraying water does not improve the layer's malleability, especially for a set-on-demand mix after 40 min. Therefore, the ideal way to obtain maximum interlayer bond strength is to adjust the static yield strength development of the mix according to cycle time. For instance, the mix with a slow static yield strength development rate can be used to print structures with long cycle times. This can be achieved by changing the precursors ratio, hydrated lime content etc. If adjusting the static yield strength of the mix is difficult during the printing process, spraying water shortly before depositing the new layer can be preferred.

## 5. Feasibility analysis and future studies

The feasibility analysis of the studied set-on-demand approach was conducted by in-line activation of the mix with the optimum hydrated lime dosage of 1 wt% (0.49S-0.26W-0.01CH) using a prototype print head mixer as shown in Fig. 11. The print head mixer contains 6 adjustable fins, which can be oriented in various inclination angles to control the extrusion rate in addition to mixing efficiency. It is worth mentioning here that the print head mixer does not contain an auger, therefore, the extrusion rate is controlled via pumping pressure and the fins. Ideally, the volume of the print head mixer should ensure a residence time of 30 s to mimic the print head mixing. The current prototype print head mixer, especially at a high extrusion rate, has a residence time lower than 30 s. However, a past study [16] has found that the required residence time for uniform mixing could be decreased by increasing the mixing speed. Therefore, a high-shear mixer was used to obtain uniform mixing at a lower residence time. The base mix is pumped using a screw pump, whereas the activator solution is pumped using a peristaltic pump. These pumps are calibrated before printing to understand the mass flow rate of the base mix and the activator solution into the print head for each speed number provided in the pump. Once the pumps are calibrated, the mass flow rates (or speed number) are selected to achieve the required activator-to-base mix ratio at the print head.

Fig. 11 (a) and (b) show the extrusion of the mix before and after in-

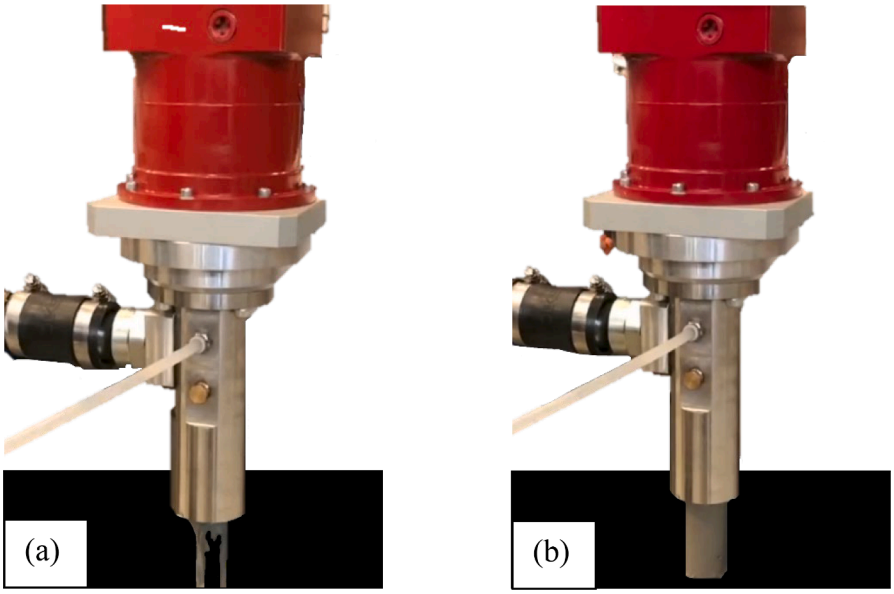


**Fig. 11.** Extrusion of geopolymer concrete (a) before and (b) after in-line activation. The test was conducted with mix 0.49S-0.26W-0.01CH.

line activation respectively. Prior to the activation (Fig. 11(a)), the extruded mix showed free flow behaviour without retaining the shape of the nozzle since the viscosity and yield strength of the mix is low before activation (discussed in section 4.3). However, shortly after the activation (Fig. 11 (b)), the mix retains the shape of the nozzle due to high yield strength (discussed in section 4.2). While the contradictory rheological behaviour observed before and after in-line activation of the geopolymer mix proves the set-on-demand approach to be feasible, the print head mixer needs to be further developed to print large structures.

In future, the print head mixer will be firmly attached to the existing 6-axis gantry-style concrete 3D printer. Furthermore, the print head mixer and pumps will be connected to the 3D printer's control system such that the mixing speed and pumping rates can be easily controlled. It is important to note that with increasing printing speed the pumping rates of the base mix and activator solution need to increase simultaneously to attain the required extrusion rate for uniform printing of layers (without tearing). Meanwhile, an increment in the pumping rates reduces the residence time of the two components in the print head mixer, which in turn reduces the mixing efficiency. Therefore, the mixing speed must be simultaneously increased to attain uniform mixing at short residence times, i.e. at fast printing rates. The relationship between the printing rates, pumping rates and mixing speed will be identified and implemented to design automation of these parameters.

## 6. Conclusion

This study investigated the effect of hydrated lime on the fresh and hardened properties of set-on-demand geopolymer concrete for 3DCP applications. Two mix design groups with varying precursor ratios (fly ash and slag) were considered with the hydrated lime dosage ranging from 0 to 8.5 wt% of the precursors. Based on the experimental study, the following conclusions can be drawn:

1. The addition of hydrated lime (CH) at small dosages in set-on-demand geopolymer concrete showed dramatic improvement in the immediate static yield strength development. However, the optimum dosage is highly dependent on the print head mixing duration. The current mix design shows 1 wt% CH as the optimum dosage and a further increase in CH dosage results in a drop in the static yield strength development.
2. The pumpability of the base mix was affected due to the cementitious properties of the slag. Therefore, the mix with 50 wt% fly ash was identified as suitable for the formulation of set-on-demand geopolymer concrete. As the base mix only contained 1 wt% hydrated lime, its effect on the pumpability of the mix was negligible.
3. In the presence of hydrated lime, the introduction of superplasticiser (which is usually incompatible with traditional geopolymer concrete) assisted in reducing the water-to-binder ratio of set-on-demand geopolymer concrete. This resulted in an enhanced 1-day compressive strength of ~ 20 MPa (~100% increment) with the highest static yield strength development.
4. Due to rapid setting, the interlayer bond strength of the specimens printed using the developed set-on-demand geopolymer concrete was reduced by 63% when the cycle time was increased from 5 s to 40 min. However, the surface spraying process minimised the strength loss to 15%.
5. The feasibility of the developed set-on-demand geopolymer concrete was analysed by using a prototype print head mixer. The contradicting rheological properties required for 3DCP were achieved by the current in-line activation method containing the proposed additives.

## CRediT authorship contribution statement

**Shravan Muthukrishnan:** Writing – original draft, Visualization, Validation, Methodology, Investigation, Data curation, Conceptualization. **Sayanthan Ramakrishnan:** Writing – review & editing, Validation, Supervision, Project administration, Conceptualization. **Jay Sanjayan:** Writing – review & editing, Supervision, Resources, Funding acquisition, Conceptualization.

## Declaration of Competing Interest

The authors declare that they have no known competing financial interests or personal relationships that could have appeared to influence the work reported in this paper.

## Data availability

Data will be made available on request.

## Acknowledgements

The Authors acknowledge Australian Research Council Grants

LE170100168, and Discovery Early Career Researcher Award of DE190100646 for the financial support to conduct the research reported in this paper.

## References


[1] Y. Chen, Y. Zhang, B.o. Pang, D. Wang, Z. Liu, G. Liu, Steel fiber orientational distribution and effects on 3D printed concrete with coarse aggregate, Mater. Struct. 55 (3) (2022).

[2] S. Muthukrishnan, S. Ramakrishnan, J. Sanjayan, Technologies for improving buildability in 3D concrete printing, Cem. Concr. Compos. 122 (2021) 104144.

[3] Y. Tao, et al., Stiffening control of cement-based materials using accelerators in inline mixing processes: Possibilities and challenges, Cem. Concr. Compos. 119 (2021), 103972.

[4] L. Reiter, et al., Setting on demand for digital concrete–Principles, measurements, chemistry, validation, Cem. Concr. Res. 132 (2020), 106047.

[5] F. Boscaro, E. Quadranti, T. Wangler, S. Mantellato, L. Reiter, R.J. Flatt, Eco-friendly, set-on-demand digital concrete, 3D Printing Addit. Manufact. 9 (1) (2022) 3–11.

[6] Y. Tao, et al., Mechanical and microstructural properties of 3D printable concrete in the context of the twin-pipe pumping strategy, Cem. Concr. Compos. 125 (2022), 104324.

[7] Y. Tao, et al., Twin-pipe pumping strategy for stiffening control of 3D printable concrete: from transportation to fabrication, Cem. Concr. Res. 168 (2023), 107137.

[8] S. Bhattacherjee, M. Santhanam, Investigation on the effect of alkali-free aluminium sulfate based accelerator on the fresh properties of 3D printable concrete, Cem. Concr. Compos. 130 (2022), 104521.

[9] S. Ramakrishnan, S. Kanagasuntharam, J. Sanjayan, In-line activation of cementitious materials for 3D concrete printing, Cem. Concr. Compos. 131 (2022), 104598.

[10] L. Shao, et al., A novel method for improving the printability of cement-based materials: Controlling the releasing of capsules containing chemical admixtures, Cem. Concr. Compos. 128 (2022), 104456.

[11] M.K. Mohan, A.V. Rahul, K. Van Tittelboom, G. De Schutter, Rheological and pumping behaviour of 3D printable cementitious materials with varying aggregate content, Cem. Concr. Res. 139 (2021) 106258.

[12] H. Zhong, M. Zhang, 3D printing geopolymers: A review, Cem. Concr. Compos. 128 (2022) 104455.

[13] M.H. Raza, R.Y. Zhong, M. Khan, Recent advances and productivity analysis of 3D printed geopolymers, Addit. Manuf. 52 (2022) 102685.

[14] M.H. Raza, R.Y. Zhong, A sustainable roadmap for additive manufacturing using geopolymers in construction industry, Resour. Conserv. Recycl. 186 (2022), 106592.

[15] S. Muthukrishnan, S. Ramakrishnan, J. Sanjayan, Effect of microwave heating on interlayer bonding and buildability of geopolymer 3D concrete printing, Constr. Build. Mater. 265 (2020), 120786.

[16] S. Muthukrishnan, S. Ramakrishnan, J. Sanjayan, Set on demand geopolymer using print head mixing for 3D concrete printing, Cem. Concr. Compos. 128 (2022), 104451.

[17] S. Muthukrishnan, S. Ramakrishnan, J. Sanjayan, In-line activation of geopolymer slurry for concrete 3D printing, Cem. Concr. Res. 162 (2022), 107008.

[18] C. Shi, R. Day, Early strength development and hydration of alkali-activated blast furnace slag/fly ash blends, Adv. Cem. Res. 11 (4) (1999) 189–196.

[19] A. Adesina, Influence of various additives on the early age compressive strength of sodium carbonate activated slag composites: An overview, J. Mech. Behav. Mater. 29 (1) (2020) 106–113.

[20] M. Kovtun, E.P. Kearsley, J. Shekhovtsova, Chemical acceleration of a neutral granulated blast-furnace slag activated by sodium carbonate, Cem. Concr. Res. 72 (2015) 1–9.

[21] J. He, et al., Influence of hydrated lime on mechanical and shrinkage properties of alkali-activated slag cement, Constr. Build. Mater. 289 (2021), 123201.

[22] Keulen, A., et al., *Working mechanism of a polycarboxylate superplasticizer in alkali-activated slag-fly ash blends.* PERFORMANCE OF ADMIXTURE AND SECONDARY MINERALS IN ALKALI ACTIVATED CONCRETE: p. 31.

[23] S. Muthukrishnan, S. Ramakrishnan, J. Sanjayan, Effect of alkali reactions on the rheology of one-part 3D printable geopolymer concrete, Cem. Concr. Compos. 116 (2021), 103899.

[24] X. Ouyang, Y. Ma, Z. Liu, J. Liang, G. Ye, Effect of the sodium silicate modulus and slag content on fresh and hardened properties of alkali-activated fly ash/slag, Minerals 10 (1) (2019) 15.

[25] H. Taghvayi, K. Behfarnia, M. Khalili, The effect of alkali concentration and sodium silicate modulus on the properties of alkali-activated slag concrete, J. Adv. Concr. Technol. 16 (7) (2018) 293–305.

[26] *PQ® Sodium Silicates*. Available from: https://www.pqcorp.com/docs/default-source/recommended-literature/pq/sodium-silicate-solids/sodiumsilicates.pdf?sfvrsn=394ebc05_3.

[27] M. Chi, R. Huang, Binding mechanism and properties of alkali-activated fly ash/slag mortars, Constr. Build. Mater. 40 (2013) 291–298.

[28] I. Ismail, S.A. Bernal, J.L. Provis, S. Hamdan, J.S.J. van Deventer, Microstructural changes in alkali activated fly ash/slag geopolymers with sulfate exposure, Mater. Struct. 46 (3) (2013) 361–373.

[29] K.A.M. El-Naggar, S.K. Amin, S.A. El-Sherbiny, M.F. Abadir, Preparation of geopolymer insulating bricks from waste raw materials, Constr. Build. Mater. 222 (2019) 699–705.

[30] F. Collins, J.G. Sanjayan, Workability and mechanical properties of alkali activated slag concrete, Cem. Concr. Res. 29 (3) (1999) 455–458.

[31] C. Shi, Steel slag—its production, processing, characteristics, and cementitious properties, J. Mater. Civ. Eng. 16 (3) (2004) 230–236.

[32] D. Feys, J.E. Wallevik, A. Yahia, K.H. Khayat, O.H. Wallevik, Extension of the Reiner-Riwlin equation to determine modified Bingham parameters measured in coaxial cylinders rheometers, Mater. Struct. 46 (1-2) (2013) 289–311.

[33] T. Marchment, J.G. Sanjayan, B. Nematollahi, M. Xia, Interlayer strength of 3D printed concrete: influencing factors and method of enhancing, in: 3D Concrete Printing Technology, Elsevier, 2019, pp. 241–264.

[34] P. Chindaprasirt, P. De Silva, S. Hanjitsuwan, Effect of high-speed mixing on properties of high calcium fly ash geopolymer paste, Arab. J. Sci. Eng. 39 (8) (2014) 6001–6007.

[35] S.H. Bong, et al., Properties of one-part geopolymer incorporating wollastonite as partial replacement of geopolymer precursor or sand, Mater. Lett. 263 (2020), 127236.

[36] X. Gao, Q. Yu, H. Brouwers, Properties of alkali activated slag–fly ash blends with limestone addition, Cem. Concr. Compos. 59 (2015) 119–128.

[37] S. Aydın, A ternary optimisation of mineral additives of alkali activated cement mortars, Constr. Build. Mater. 43 (2013) 131–138.

[38] N. Puthipad, M. Ouchi, S. Rath, A. Attachaiyawuth, Enhancement in self-compactability and stability in volume of entrained air in self-compacting concrete with high volume fly ash, Constr. Build. Mater. 128 (2016) 349–360.

[39] R. Jayathilakage, P. Rajeev, J. Sanjayan, Yield stress criteria to assess the buildability of 3D concrete printing, Constr. Build. Mater. 240 (2020), 117989.

[40] G.M. Moelich, J. Kruger, R. Combrinck, Modelling the interlayer bond strength of 3D printed concrete with surface moisture, Cem. Concr. Res. 150 (2021), 106559.

[41] J.G. Sanjayan, B. Nematollahi, M. Xia, T. Marchment, Effect of surface moisture on inter-layer strength of 3D printed concrete, Constr. Build. Mater. 172 (2018) 468–475.

[42] A.J. Babafemi, J.T. Kolawole, M.J. Miah, S.C. Paul, B. Panda, A concise review on interlayer bond strength in 3d concrete printing, Sustainability 13 (13) (2021) 7137.